

PAPER

## Dynamics and chemical mode analysis of plasma thermal-chemical instability

To cite this article: Hongtao Zhong *et al* 2021 *Plasma Sources Sci. Technol.* **30** 035002

View the [article online](#) for updates and enhancements.

### You may also like

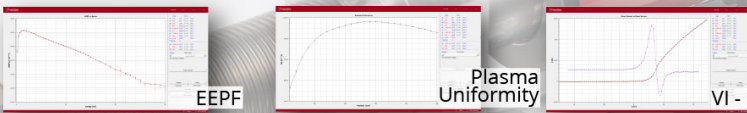
- [A Kinetic Study of the Chemical Vapor Deposition of Silicon Carbide from Dichlorodimethylsilane Precursors](#)  
T. Takeuchi, Y. Egashira, T. Osawa *et al.*
- [Monsanto Chemical Co.—ECS Sustaining Member](#)
- [Experimental Verification of a Fundamental Model for Multiwafer Low pressure Chemical Vapor Deposition of Polysilicon](#)  
Thomas A. Badgwell, Thomas F. Edgar, Isaac Trachtenberg *et al.*



### Intelligent Sensors for Plasma Monitoring and Diagnostics

**“The most advanced Langmuir Probe on the market”**

Measures the characteristics of the bulk plasma region with an 80 MHz sampling rate. Pulse profiling and single shot plasmas can be measured with unrivalled time resolution.



**Applications:**

- RF-driven Plasmas
- Pulsed Plasma
- Atmospheric Plasma
- Magnetron Sputtering

**Measures:**

- EEDF
- Plasma Density
- Plasma & Floating Potential
- Electron Temperature

[LEARN MORE](#)  
[www.impedans.com](http://www.impedans.com)

# Dynamics and chemical mode analysis of plasma thermal-chemical instability

Hongtao Zhong\* , Mikhail N Shneider , Xingqian Mao ,  
and Yiguang Ju

Department of Mechanical and Aerospace Engineering, Princeton University, Princeton, NJ 08544, United States of America

E-mail: [hongtaoz@princeton.edu](mailto:hongtaoz@princeton.edu)

Received 31 October 2020, revised 9 December 2020

Accepted for publication 20 January 2021

Published 15 March 2021



CrossMark

## Abstract

The stability of the weakly ionized plasma and the transition from a stable homogeneous discharge to unstable filaments play an important role in gas laser physics, plasma-assisted combustion, chemical reforming, and material synthesis. Theoretical stability analysis and thermal-chemical mode analysis were performed to understand the mechanism of plasma thermal-chemical instability by using a zero-dimensional plasma system with both simplified and detailed chemical kinetics of H<sub>2</sub>/O<sub>2</sub>/N<sub>2</sub> mixtures. The plasma dynamic and kinetic models accounted for multiple physical mechanisms in the chemically-reactive weakly ionized plasma, including ionization, attachment/detachment, recombination, vibrational and electronic energy relaxation, convective and diffusive species/heat removal, Joule heating, and detailed chemical kinetics. An analytical criterion and the explosive mode species/temperature pointers were formulated while the representative active species were identified for different thermal-chemical modes. The results showed that in addition to the classical thermal-ionization mechanism, various chemical modes from chemical heat imbalance and elementary kinetics significantly modified the time dynamics and the stability of the weakly ionized plasma. The present analysis provides insights and guidance to control plasma instability using chemical kinetics.

Keywords: plasma thermal-chemical instability, weakly ionized plasma, chemically-reactive flow, stability analysis, chemical mode analysis

 Supplementary material for this article is available [online](#)

(Some figures may appear in colour only in the online journal)

## Nomenclature

[ ]<sub>s</sub> Steady state quantities

δ[ ] Perturbed quantities

[ ] Mixture-averaged quantities

[ ] Logarithmic normalized quantities

$\beta_{ep}$  Electron-ion recombination coefficient, cm<sup>3</sup> s<sup>-1</sup>

$\beta_{ii}$  Ion-ion recombination coefficient, cm<sup>3</sup> s<sup>-1</sup>

**g** Source term in a general differential equation system

**J** Jacobian matrix of **g**

**k** Propagation constant, cm<sup>-1</sup>

**y** N-dimensional column vector for a general differential equation system

$\eta_T$  Fraction of Joule heat responsible for direct heating

$\eta_V$  Fraction of Joule heat responsible for vibrational excitation

$\gamma$  Mixture-averaged specific heat ratio

$\hbar\omega$  Vibrational quanta, eV

$\lambda$  Eigenvalue of the Jacobian matrix, s<sup>-1</sup>

$\mathcal{L}$  Spatial operator for convection, drift and diffusion

$\mathcal{O}()$  At the order of

$\mu_e$  Electron mobility, cm<sup>2</sup> V<sup>-1</sup> s<sup>-1</sup>

$\mu_n$  Negative ion mobility, cm<sup>2</sup> V<sup>-1</sup> s<sup>-1</sup>

\* Author to whom any correspondence should be addressed.

$\mu_p$  Positive ion mobility,  $\text{cm}^2 \text{V}^{-1} \text{s}^{-1}$   
 $\nu_a$  Attachment rate,  $\text{s}^{-1}$   
 $\nu_d$  Detachment rate,  $\text{s}^{-1}$   
 $\nu_i$  Ionization rate,  $\text{s}^{-1}$   
 $\nu_j$  Joule heating rate,  $\text{s}^{-1}$   
 $\nu_\beta$  Electron-ion recombination rate,  $\text{s}^{-1}$   
 $\nu_{\text{conv}}$  Species/Heat removal rate,  $\text{s}^{-1}$   
 $\nu_c$  Chemical heat releasing/absorption rate,  $\text{s}^{-1}$   
 $\omega$  Cyclic frequency,  $\times 2\pi \text{s}^{-1}$   
 $\omega_i$  Total reaction rate of the species  $i$ , molecule  $\text{cm}^{-3} \text{s}^{-1}$   
 $\omega_{ij}$  Reaction rate of the species  $i$  in reaction  $j$ , molecule  $\text{cm}^{-3} \text{s}^{-1}$   
 $\Pi_{\text{VV}}$  Energy flow of vibrational quanta in the vibrational domain,  $\text{J cm}^{-3} \text{s}^{-1}$   
 $\sigma$  Conductivity,  $\Omega^{-1} \text{cm}^{-1}$   
 $\tau$  Convective/diffusive flow time scale, s  
 $\tau_{\text{VT}}$  Vibrational-translational (V-T) relaxation time scale,  $= 1/\nu_{\text{VT}}$ , s  
 $c_p$  Specific heat,  $\text{J K}^{-1}$   
 $E$  Electric field,  $\text{V cm}^{-1}$   
 $E/N$  Reduced electric field, Td  
 $E_v$  Vibrational energy,  $\text{eV cm}^{-3}$   
 $E_v^0$  Equilibrium vibrational energy,  $\text{eV cm}^{-3}$   
 $f_i$  Thermal-chemical mode corresponding to the eigenvalue  $\lambda_i$   
 $H$  Enthalpy of the mixture at gas temperature  $T_g$ ,  $\text{J mol}^{-1}$   
 $H_0$  Enthalpy of the mixture at the ambient temperature  $T_0$ ,  $\text{J mol}^{-1}$   
 $h_i$  Enthalpy of the species  $i$ ,  $\text{J mol}^{-1}$   
 $I$  Current, mA  
 $i_{\text{max}}$  Total species number  
 $j_c$  current density,  $\text{mA cm}^{-2}$   
 $j_c E$  Joule heating,  $\text{J cm}^{-3} \text{s}^{-1}$   
 $j_{\text{max}}$  Total reaction number  
 $k$  Boltzmann constant,  $\text{J K}^{-1}$   
 $N$  Gas number density,  $\text{cm}^{-3}$   
 $N_0$  Ambient gas number density,  $\text{cm}^{-3}$   
 $n_e$  Electron number density,  $\text{cm}^{-3}$   
 $N_i$  Gas number density of species  $i$ ,  $\text{cm}^{-3}$   
 $n_n$  Negative ion number density,  $\text{cm}^{-3}$   
 $n_p$  Positive ion number density,  $\text{cm}^{-3}$   
 $p$  Pressure, Torr  
 $Q_c$  Chemical heat release/absorption,  $\text{J cm}^{-3} \text{s}^{-1}$   
 $Q_c^V$  Chemical heat release/absorption pumped into the vibrational energy,  $\text{J cm}^{-3} \text{s}^{-1}$   
 $S$  Cross section of the plasma volume,  $\text{cm}^2$   
 $T_0$  Ambient gas temperature, K  
 $T_e$  Electron energy, eV  
 $T_g$  Gas translational temperature, K  
 $T_v$  Gas vibrational temperature, K  
 $x_i$  Mole fraction of the species  $i$   
 CSP Computational singular perturbation  
 NDC Negative differential conductivity  
 RAS Representative active species  
 SP Species/temperature pointer  
 TCM Thermal-chemical modes  
 TCMA Thermal-chemical mode analysis

## 1. Introduction

Weakly ionized gas plasma has been widely used in various plasma applications including high-energy gas lasers [1–4], geophysics [5, 6], plasma-assisted combustion [7–9], plasma-assisted chemical synthesis and material manufacturing [10–12]. The operating conditions are maintained by means of electric current flowing in a gas mixture under electric or electromagnetic fields. Heat/species diffusion/convection, volumetric energy transfer as well as the chemical processes involving charged and excited particles formation and interactions all contribute to the rich dynamics and different states of the weakly ionized gas plasma.

The homogeneous and contracted/constricted states are two commonly-seen weakly ionized plasma states. In the former one, plasma is distributed uniformly within a large volume and resistant to perturbations. Energetic electrons, excited species and neutral species are in non-equilibrium. While in the latter one, inhomogeneous filaments are formed with much higher degrees of ionization and local gas temperature. Electrons and neutral species are closer to the equilibrium. The transition from the homogeneous non-equilibrium plasma discharge to filamentary near-equilibrium hot channels at sufficiently high energy inputs or enhanced pressures is critically important for its vast applications. To name a few, in molecular gas lasers (e.g. CO<sub>2</sub> and CO lasers), the transition from homogeneous states to contracted states will seriously erode the power capacity and optical quality of the active medium [2–4]. In plasma-assisted combustion, the homogeneous states will have prominent chemical effects and facilitate volumetric ignition due to its high electron energy, while the contracted states will have dominant thermal effects to force local ignition via its high gas temperature [13]. In plasma-assisted chemical manufacturing, thin filaments, formed through contraction of a diffuse-like discharge, will have less efficiency and selectivity and may reduce the lifetime and chemical functionality of the catalysts. Moreover, from the viewpoint of fundamental research of plasma, the physical and chemical mechanisms behind the transition are also of interest. The contraction phenomenon provides one of the illustrative examples for the macroscopic self-organization of a gas plasma [14] as a consequence of mutual nonlinear influences of a variety of processes proceeding at a microscopic level. As such, there is a great need to perform stability and reaction kinetic analysis to better understand the criterion for transitions between the homogeneous and filamentary states involving plasma dynamics and elementary reactions and further optimize the performance of related devices.

The classical theoretical analysis for this homogeneous-filamentary-transition, known as ‘plasma thermal instability’, could be traced back to 1960–1980s [15–18]. The positive feedback of the thermal-ionization mechanism is expressed as,

$$T_g \uparrow \rightarrow N \downarrow \rightarrow E/N \uparrow \rightarrow T_e \uparrow \rightarrow \nu_i(T_e) \uparrow \rightarrow n_e \uparrow \rightarrow j_c E \uparrow \rightarrow T_g \uparrow. \quad (1)$$

From equation (1), at isobaric conditions, any local temperature rise will lower the gas number density ( $N$ ) and further increase the reduced electric field ( $E/N$ ). As a result,

the ionization rates controlled by  $E/N$  will increase. Faster ionization rates lead to higher production rates of electrons and more Joule heating. Later, more physical insights including the non-equilibrium electron distribution over velocities, ambipolar diffusion and the volumetric electron recombination were discussed in details for their influences on the transition [19]. Both experimental work [19] and numerical modeling [20, 21] for the contraction showed that the transition had a hysteresis cycle. Under some external discharge parameters, both homogeneous and contracted states could co-exist. By applying a sufficient perturbation, the homogeneous plasma could abruptly transform into a contracted state. However, previous studies of plasma thermal instability were mostly limited to noble gases, air [15, 18, 19, 21, 22] or mixtures in gas lasers [2–4]. How plasma instability would occur in chemically-reactive mixtures is not well understood.

Recently Zhong *et al* [23, 24] proposed a new concept of plasma thermal-chemical instability to address the positive feedback and couplings between plasma and plasma-enhanced chemical reactions in the reactive flow. With simulations of the dynamics of a self-sustained glow discharge in a reactive  $H_2-O_2-N_2$  mixture, it was demonstrated that both the heat release/absorption and  $H_2-O_2$  chemical kinetics affected the critical plasma current for the transition between the homogeneous and the contracted states. This concept of plasma thermal-chemical instability has been validated in several experimental studies. Wolf *et al* [25] and Viegas *et al* [26] described the characteristic discharge modes in a  $CO_2$  microwave plasma and showed the coupling between the classical thermal-ionization instability and thermally-driven endothermic  $CO_2$  dissociation reactions. Rouso *et al* [27] performed ICCD imaging and measured 1D time-resolved *in situ* electric field in a nanosecond pulsed dielectric barrier discharge plasma of  $O_2-Ar$  mixtures with and without  $CH_4$  (fuel) addition. They found that the rapid formation of streamers from an originally uniform discharge appeared to be caused by the chemical kinetics of plasma-assisted low temperature  $CH_4$  oxidation. These results again highlighted the impact of chemical kinetics on the contraction phenomena of reactive molecular gas plasmas. However, how such a thermal-chemical instability initiates and how the character of the governing differential equations transit from one stable homogeneous solutions into another unstable filamentary solutions in accordance with not only discharge parameters but also chemical kinetics parameters are not understood well. In addition, it is not clear which reactions or species contribute to what extent to the growth of the unstable modes of the plasma instability.

Transitions and critical conditions for the weakly ionized plasma have been discussed for decades [1, 16, 28]. Mathematically, it is equivalent to the stability analysis of a system of differential equations consisting of species/energy balance equations as

$$\frac{\partial \mathbf{y}}{\partial t} + \mathcal{L}(\mathbf{y}) = \mathbf{g}(\mathbf{y}). \quad (2)$$

The unknowns in the target system are denoted as an  $N$ -dimensional column vector  $\mathbf{y}$  as a function of time and spatial variables.  $\mathbf{g}$  is the source term and  $\mathcal{L}(\mathbf{y})$  is the spatial operator for convection, drift and diffusion. The system can

be linearized by substituting expressions as  $\mathbf{y} = \mathbf{y}_0 + \delta \mathbf{y}$  for unknowns and assuming that the perturbations  $\delta \mathbf{y}$  are small. The solution of the linearized system is sought in the form of plane waves as  $\delta \mathbf{y} = \mathbf{y}_0 e^{i(\mathbf{k} \cdot \mathbf{x} - \omega t)}$ , which yields a system of  $n$  algebraic equations involving steady-state values  $\mathbf{y}_0$ . Setting the determinant of the system to zero yields the dispersion relations involving propagation constant  $\mathbf{k}$ , frequency  $\omega$  and other physical parameters as

$$D(\omega, \mathbf{k}) = 0. \quad (3)$$

If at least one of the  $n$  complex roots satisfies  $\text{Im}(\omega) > 0$  at a given  $\mathbf{k}$ , perturbations will grow exponentially. The critical condition for the system to become linearly unstable corresponds to

$$\max[\text{Im}(\omega(\mathbf{k}))] = 0 \quad (4)$$

which physically represents the transition between contracted (unstable,  $\max[\text{Im}(\omega)] > 0$ ) and homogeneous (stable,  $\max[\text{Im}(\omega)] < 0$ ) plasma states. Under the zero-dimensional assumption ( $\mathcal{L}(\mathbf{y}) = 0, \mathbf{k} = 0$ ), the above analysis is equivalent to compute the eigenvalues  $\lambda$  of the Jacobian matrix of the source term  $\mathbf{g}$ , defined as

$$\mathbf{J} = \frac{\partial \mathbf{g}}{\partial \mathbf{y}}. \quad (5)$$

The conversion between  $\lambda$  and  $\omega$  is  $\lambda = -i\omega$ . Then equation (4) is equivalent to

$$\max[\text{Re}(\lambda)] = 0. \quad (6)$$

For the consistency with previous analysis on chemical modes [29, 30], we stick to the notation of equation (6) for the critical conditions in the following content. However, the methodology is mathematically equivalent with equation (4) and previous analysis on plasma waves and instabilities [1, 28]. For simplified systems with a reduced number of species, the critical conditions can be derived by hand to gain the physical and chemical insights. For realistic systems with detailed chemistry, such dependence of the stability on the species and reactions is often computed numerically using numerical perturbation. By inspection of the numerical data, reaction modes and sensitivity of individual reactions and species towards the plasma thermal-chemical instability can be further discussed [29].

The objective of this work is to analyze the stability of weakly ionized plasma in the presence of chemical kinetics to gain insights on the control of plasma thermal-chemical instability. The paper is structured as the following: in section 2, both a general formulation with detailed chemistry and a self-consistent model with simplified chemistry are provided to describe the dynamics of the thermal-chemical instability for reactive plasmas and the foundations for the stability analysis are laid. In section 3, the stability criterion and chemical modes of such a reacting system are derived analytically under simplified kinetics or computed numerically under detailed kinetics. The explosive modes and their ‘representative active species’ (RAS) associated with elementary kinetics for plasma thermal-chemical instability are presented. The influence

of different physical-chemical mechanisms including heat addition/absorption, vibrational-translation relaxation, attachment/detachment and elementary kinetics on the stability of a reactive plasma system is investigated. Finally, conclusions and future work are provided in section 4.

## 2. Zero-dimensional plasma model

The transitions from homogeneous to filamentary plasma states have been demonstrated in different low temperature plasma power sources [13, 20, 25, 27]. To simplify the plasma kinetic modeling and remain the generality of the plasma thermal-chemical instability, the discussion below is limited to a DC glow discharge in the mixture of molecular gases. The extension of such analysis to other discharges can be done in a similar way. These plasmas in the positive column of the glow discharge are characterized by pressures of 10–300 Torr, relatively low electron energy ( $\sim 1$  eV), and low ionization degree (below  $10^{-6}$ ). The general behavior of such a plasma is governed by an exceedingly complex network of energy transfer and chemical interactions [16] and requires an extensive multidimensional description. Nevertheless, previous numerical simulations [2, 16, 31] have shown that to determine the dominant mechanisms corresponding to a particular circumstance, assumptions should be made which match related time scales, retain essential physical features while greatly reducing the complexity of the analysis.

On the basis of such considerations, we assume that the instability grows from the initially homogeneous plasma. Under those assumptions, we simplify the problem as zero-dimensional. This zero-dimensional assumption will be further examined in section 3.4 and validated with previous one-dimensional results [20, 21, 23, 24]. A demonstration figure of zero-dimensional stability analysis is shown in figure 1, where we consider  $H_2-O_2-N_2$  chemistry and separate the contracted states and the homogeneous states by their different gas temperatures, discharge power inputs and active species. In this section, a general formulation for detailed kinetics and a simplified model with reduced kinetics for the zero-dimensional plasma system will be presented. In addition, the methodology for analytical/numerical perturbation will also be introduced briefly.

### 2.1. A general zero-dimensional formulation

The general zero-dimensional formulation consists of a system of ordinary differential equations for species and temperature as

$$\frac{dN_i}{dt} = \sum_{j=1}^{j_{\max}} \omega_{ij}(t) - \frac{N_i}{\tau} \quad (i = 1, 2, 3, \dots, i_{\max}) \quad (7)$$

$$\frac{\gamma}{\gamma - 1} k \frac{d(NT_g)}{dt} = j_c E - \frac{3}{2} k \frac{d(n_e T_e)}{dt} - \sum_i^{i_{\max}} h_i \frac{dN_i}{dt} - \frac{H - H_0}{\tau}, \quad (8)$$

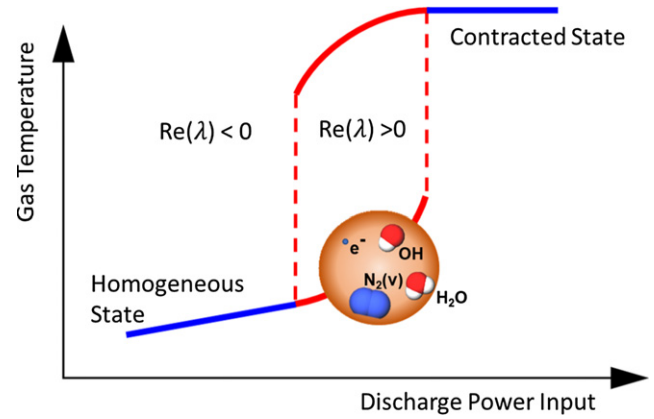


**Figure 1.** The schematic of zero-dimensional stability analysis of plasma thermal-chemical instability in the  $H_2-O_2-N_2$  system. Under low plasma current, the homogeneous plasma volume remain stable (shown as the blue lower branch). With increased energy input (above some criticality), perturbations through the plasma system will self-amplify and rich kinetics and dynamics are expected (shown as the transition region in red). Eventually the system will transit to the contracted state (shown as the upper branch) through non-equilibrium energy transfer and plasma-assisted chemical pathways.

where  $i$  is the species index in the chemical mechanism and  $N_i$  is the number density of species  $i$ .  $\omega_{ij}$  is production or consumption rate of species  $i$  contributed by reaction  $j$ .  $i_{\max}$  and  $j_{\max}$  are the total numbers of species and reactions in the chemical mechanism.  $\tau$  is the characteristic time for the effective removal of charged particles and energy by convection and diffusion transport. It is frequently used in theoretical studies to make the zero-dimensional calculations more tractable. The formulation of gas translational temperature  $T_g$  is similar with Flitti and Pancheshnyi's method [32]. The total electric power ( $j_c E$ ) is distributed into four parts: the translational degree of freedom of electrons, the translational degree of freedom of gas, the internal degree of freedom of gas and the convective loss.  $\gamma$  is the mixture-averaged specific heat ratio and  $h_i$  is the specific enthalpy of species  $i$ .  $H$  is the enthalpy of the mixture at the temperature  $T_g$  while  $H_0$  is the enthalpy of the same mixture at the ambient temperature  $T_0$ . The current density  $j_c$  in the total electric power term is defined as  $j_c = e(\mu_e n_e + \mu_n n_n + \mu_p n_p)E$ . The chemical mechanism following this formulation should include relevant reactions such as electron-impact reactions (excitation, dissociation, attachment and ionization), quenching/relaxation reactions of vibrationally/electronically excited states, charged species interactions (detachment, charge exchange, electron-ion and ion-ion recombination) and elementary chemical kinetics of molecules and radicals. The gas heating from all the above-mentioned reactions is considered for the time evolution of the gas translational temperature.

Two auxiliary relations are used to couple the whole system. One relates external current, conductivity and electric field as

$$E(t) = \frac{I}{\sigma(t)S}. \quad (9)$$

Here the discharge current,  $I$ , determined by the external electric circuit and defined as a parameter, can be related with electric field  $E(t)$ , conductivity  $\sigma(t)$ , which is calculated as  $e(\mu_e n_e + \mu_n n_n + \mu_p n_p)$ , and characteristic cross section of the zero-dimensional plasma volume  $S$ . The other is the ideal gas assumption as

$$p = \sum_i N_i kT_g, \quad (10)$$

where  $\sum_i N_i$  is a summation of the neutral and ion species. The contribution from electrons is neglected as  $n_e \ll \sum_i N_i$  is satisfied in the weakly ionized plasma. The discussion is further limited to isobaric conditions. Equations (7)–(10) form a general zero-dimensional formulation for the thermal-chemical instability, consistent with previous investigations in plasma assisted ignition and plasma-combustion kinetic studies [33].

The above formulations are implemented numerically in this work. The plasma chemistry library ZDPlasKin [34] and the chemical kinetics library CHEMKIN [35] are integrated using a time-splitting numerical scheme [33, 36, 37]. The electron energy distribution function (EEDF) and the rate coefficients of electron-impact reactions are calculated by a Boltzmann equation library BOLSIG+ [38]. The cross sections of electron-impact reactions are obtained from the LXCat Project [39] and more details are provided in supplementary material (<https://stacks.iop.org/PSST/30/035002/mmedia>). For the demonstrative example as the plasma thermal-chemical instability in the  $H_2-N_2-O_2$  mixture in section 3, the chemical mechanism includes 62 species, 151 elementary reactions and 666 plasma reactions. 69 electron-impact reactions are considered for the EEDF calculation. This  $H_2-O_2-N_2$  combustion mechanism is developed from Princeton HP-MECH [40]. The sub-mechanism of  $NO_x$  is from [37]. Excited and charged species in the mechanism include  $N_2(v)(v = 1-8)$ ,  $H_2(v)(v = 1-3)$ ,  $O_2(v)(v = 1-4)$ ,  $N_2(A)$ ,  $N_2(B)$ ,  $N_2(a')$ ,  $N_2(C)$ ,  $N(^2D)$ ,  $O_2(a^1\Delta_g)$ ,  $O_2(b^1\Sigma_g^+)$ ,  $O_2^*$ ,  $O(^1D)$ ,  $O(^1S)$ ,  $N_2^+$ ,  $N_4^+$ ,  $H_2^+$ ,  $H_3^+$ ,  $O_2^+$ ,  $O_4^+$ ,  $H_3O^+$ ,  $O^-$ ,  $O_2^-$ ,  $O_4^-$ ,  $OH^-$  and electron. The gas heating from reactions involving  $N_2$ ,  $O_2$  [32],  $H_2$  [41] and related radicals and plasma species are all considered. The corresponding detailed reactions are provided in the supplementary material.

## 2.2. A simplified zero-dimensional model

The above general formulations enable detailed modeling of the dynamics of the thermal-chemical instability for realistic reactive plasmas. However, complicated chemical kinetics may hinder the analytical study of the stability boundary and obscure valuable physical insights for the zero-dimensional plasma system. Therefore, a simplified zero-dimensional model with five independent variables is presented. This simplified model is consistent with our general formulation in section 2.1 given the same chemical mechanism (details are provided in the supplementary material) and more importantly, it lays foundations for the analytical investigation of the stability criterion in the next section.

The zero-dimensional simplified system is composed of charged species continuity (electron number density  $n_e$ , negative ion number density  $n_n$ , positive ion number density  $n_p$ ) and energy equation (vibrational energy ( $E_v$ ) and translational

temperature equations ( $T_g$ )) as

$$\frac{dn_e}{dt} = \bar{\nu}_i n_e - \bar{\nu}_a n_e + \bar{\nu}_d n_n - \bar{\beta}_{cp} n_e n_p - n_e / \tau \quad (11)$$

$$\frac{dn_n}{dt} = \bar{\nu}_a n_e - \bar{\nu}_d n_n - \bar{\beta}_{in} n_n n_p - n_n / \tau \quad (12)$$

$$\frac{dn_p}{dt} = \bar{\nu}_i n_e - n_p / \tau - \bar{\beta}_{cp} n_e n_p - \bar{\beta}_{in} n_n n_p - n_p / \tau \quad (13)$$

$$N\bar{c}_p \frac{dT_g}{dt} = \eta_T j_c E + \Pi_{VV} + \frac{E_v - E_v^0}{\bar{\tau}_{VT}} + Q_c - N_0 \bar{c}_p \frac{T_g - T_0}{\tau} \quad (14)$$

$$\begin{aligned} \frac{dE_v}{dt} = & \eta_v j_c E - \Pi_{VV} - \frac{E_v - E_v^0}{\bar{\tau}_{VT}} + Q_c^V \\ & - (N_0/N) \frac{E_v - E_v^0}{\tau} \end{aligned} \quad (15)$$

One must note that the number of independent variables in the simplified system can be increased, if needed. In addition, in the reactive flow, plasma kinetic parameters including ionization, attachment and detachment frequencies are all functions of the composition  $x_i$ . The notation  $[\bar{\quad}]$  is used to denote all mixture-averaged quantities in the simplified model. From equations (11)–(13), charged species are controlled by ionization, attachment/detachment, electron-ion/ion-ion recombination processes and convective removal. In the gas temperature equation [equation (14)], terms on the right-hand side represent Joule heating, energy flow of vibrational quanta in the vibrational energy domain, V–T energy relaxation, convective heat removal and the energy exchange from chemical kinetics of neutral species, denoted as  $Q_c$ . For excited plasma kinetics, only the vibrational excitation, V–V energy exchange and V–T energy relaxation are considered at the low reduced electric field ( $\leq 100$  Td) and electron energy ( $\leq 1$  eV). The vibrational energy  $E_v$  is assumed to store in one vibrational level of the diluent (e.g.  $N_2$ ) for simplification and is linked with the vibrational gas temperature  $T_v$  as  $E_v = N\hbar\omega / (\exp(\hbar\omega/kT_v) - 1)$ . On the right-hand side of equation (15), the term  $Q_c^V$  is also included, which represents the heat release or absorption of the vibrational energy from reactions such as



EEDF is not solved in this simplified system. Instead BOLSIG+ is applied in advance to generate a check-up table for  $T_e(E/N)$  relations to link reduced electric field to kinetic coefficients.

## 2.3. Perturbation analysis

The linear stability analysis starts from small wave-like departures (denoted as  $\delta[\quad]$ ) from the equilibrium values (denoted as

$[\ ]_s$ ) of the major variables. Here, perturbations of several key quantities for the plasma thermal-chemical instability are presented. First, a perturbation of the current–voltage relation in equation (9) yields

$$\frac{\delta E}{E_s} + \frac{\delta \sigma}{\sigma_s} - \frac{\delta I}{I} = 0. \quad (16)$$

According to equation (1), when the ionization is intensified, more electrons are accumulated and the conductivity builds up exponentially ( $\delta \sigma > 0$ ), leading to a drop in the electric field ( $\delta E < 0$ ) given the current is unchanged. The fluctuations from the electric field and the conductivity can further spread to the Joule heating term in the temperature equation as

$$\delta(j_c E) = (j_c E)_s \left[ \frac{\delta \sigma}{\sigma_s} + 2 \frac{\delta E}{E_s} \right]. \quad (17)$$

From the expression,  $\delta(j_c E)$  is controlled by the growth of the electron number density and hence the conductivity as well as the dropping of electric field.

Another key quantity for controlling the plasma kinetics is the reduced electric field ( $E/N$ ). The perturbed reduced electric field  $E/N$  could be written as

$$\delta \left( \frac{E}{N} \right) = \left[ \frac{E}{N} \right]_s \left[ \frac{\delta T}{T_s} + \frac{\delta E}{E_s} \right]. \quad (18)$$

Clearly two physical processes contribute to the fluctuation of  $E/N$ . One is the temperature perturbation or thermal expansion. Positive temperature perturbation ( $\delta T > 0$ ) induces positive increment of reduced electric field ( $\delta(\frac{E}{N}) > 0$ ). The other is the charge accumulation or the electric field drop. High steady-state electric field ( $E_s$ ) or temperature ( $T_s$ ) may inhibit the growth of the reduced electric field. The perturbation will further propagate from the reduced electric field to plasma kinetic processes as  $E/N$  controls the EEDF and critical processes like ionization, attachment/detachment and recombination.

The perturbed  $N$ -dimensional column vector  $\delta \mathbf{y}$  forms a linearized ordinary differential equation system. The linear stability analysis is converted into calculating matrix eigenvalues of this dynamical system. The stability boundary in the parameter space is determined by equation (4) and presented in section 3. For simplified plasma reaction systems, the steady-state stability boundary is derived analytically and the results are validated numerically by using the MATLAB symbolic toolbox.

#### 2.4. Thermal-chemical mode analysis

To better characterize the thermal-chemical instability and understand how the thermal-chemical modes and the stability behavior evolve with respect to time, for detailed plasma reaction systems, we follow the computational singular perturbation theory [29, 30] and develop the thermal-chemical mode analysis (TCMA) to analyze the stability and chemical modes of the zero-dimensional plasma system with chemical kinetics (detailed numerical implementation is introduced in supplementary material). The analysis is based on the eigenvalue

decomposition of the Jacobian matrix [defined in equation (5)] at different time moments as

$$\frac{d}{dt} \delta \mathbf{y} = \mathbf{J} \cdot \delta \mathbf{y} = \Lambda \mathbf{B} \cdot \delta \mathbf{y}. \quad (19)$$

$\Lambda$  is the diagonal matrix as  $\text{diag}(\lambda_1, \lambda_2, \dots, \lambda_N)$ .  $A$  and  $B$  are composed of column and row eigenvectors, respectively. This Jacobian matrix consists of thermal-chemical property for the system and defines thermal-chemical ‘modes’ (TCM) in the system as

$$\frac{d}{dt} f_i = \lambda_i f_i, \quad f_i = \mathbf{B} \cdot \delta \mathbf{y}, \quad i = 1, 2, \dots, N. \quad (20)$$

Eigenvalues of the Jacobian with positive real parts ( $\text{Re}(\lambda_i) > 0$ ) indicate that the system is unstable or ‘explosive’. The associated chemical modes tend to grow exponentially with the time scale of  $\lambda_i^{-1}$ . If no positive eigenvalues are present, the system is linearly resistant to perturbations and approaching the chemical equilibrium as all chemical modes tend to decay. Thus, the zero-crossing of an eigenvalue from negative to positive is the critical condition for the stability of the system [equation (6)].

To understand which species and reactions are contributing to the explosive TCMs and to further project the system stability to the species space, the concept of ‘explosive mode species/temperature pointer’ (SP) is defined, which is similar to the ‘radical pointer’ used in previous combustion kinetic studies [29, 30] as

$$\text{SP}_i = \text{diag}(\mathbf{a}_i \cdot \mathbf{b}_i) \quad i = 1, 2, \dots, N, \quad (21)$$

where  $\mathbf{a}_i$  and  $\mathbf{b}_i$  are the right and left eigenvectors, respectively, associated with  $\lambda_i$  and the chemical mode  $f_i$ . The  $k$ th entry of  $\text{SP}_i$  indicates the correlations between the  $k$ th variable in the column vector  $\mathbf{y}$  and the  $i$ th chemical mode  $f_i$ . The ‘RAS’ for the chemical mode  $f_i$  is defined as the species which has the largest SP values among all species. In other words, a certain chemical mode  $f_i$  is mostly related to the RAS.

### 3. Results and discussions

Given the above formulations, we perform perturbations around the steady states (sections 3.1, 3.2 and 3.4) or mode analysis at discrete times (section 3.3) and discuss the stability criterion or the transition caused by the thermal-chemical effects in a zero-dimensional plasma system. Specifically, eigenvalues and eigenmodes ( $\text{Re}(\lambda)$ ) are provided both at steady states or during the time evolution to consider the influence from chemical kinetics.

The  $\text{N}_2\text{--O}_2$  and  $\text{H}_2\text{--O}_2\text{--N}_2$  mixtures are mainly discussed for several reasons. First, hydrogen is a clean efficient energy carrier and widely used in plasma assisted chemical synthesis while air is the most convenient bath gas. Second, rich chemical kinetics of the  $\text{H}_2\text{--O}_2\text{--N}_2$  mixture and possible formations of  $\text{O}_3$ ,  $\text{NO}_x$ ,  $\text{H}_2\text{O}$  and  $\text{NH}_3$  have been reported previously [41, 42]. Potential couplings between the thermal-ionization mechanism and chemical kinetics are expected in this mixture. Surely the plasma thermal-chemical instability is universal and not limited to some certain species. Nevertheless, discussions of other reacting systems are beyond the scope of the this work.

The mixture is set in a preheated environment (400–800 K) for elevated chemical reactivity (consistent with previous discussions on ‘warm’ plasmas [43]). The pressures are varied from 50–250 Torr while convective time scales are varied from 1 ms–10 ms. Those values are adjusted to keep the critical current in a reasonable range (1–100 mA).

### 3.1. Eigenmodes of endothermic/exothermic reactions

The thermal effect has been discussed in the classical thermal-ionization mechanism [22] by only perturbing the gas translational energy equation [equation (14)] with negligible energy transfer from the vibrational energy ( $\eta_T \approx 1$ ,  $\Pi_{VV} \approx 0$ ). The eigenmode under those simplifications is

$$\text{Re}(\lambda) = \left( \frac{\sigma_s E_s^2}{N_0 c_p T_0} \right) \frac{\partial \ln n_{e,s}}{\partial \ln T_s} - \frac{1}{\tau} \approx \nu_J \frac{\partial \hat{\nu}_i}{\partial \left( \frac{\hat{E}}{N} \right)} - \nu_{\text{conv}}, \quad (22)$$

where  $\nu_J = \frac{\sigma_s E_s^2}{N_0 c_p T_0}$  is the Joule heating rate,  $\nu_{\text{conv}}$  is the heat removal rate, while  $\frac{\partial \hat{\nu}_i}{\partial \left( \frac{\hat{E}}{N} \right)}$  is the normalized sensitivity of the ionization frequency towards the reduced electric field. Equation (22) demonstrates the stabilization of heat removal and the destabilization by Joule heating and ionization. However, the influence of endothermic/exothermic reactions is neglected. A straightforward extension by considering chemical heat absorption/release term  $Q_c$  in equation (14) yields

$$\text{Re}(\lambda) \approx \nu_J \frac{\partial \hat{\nu}_i}{\partial \left( \frac{\hat{E}}{N} \right)} - \nu_{\text{conv}} + \nu_c. \quad (23)$$

Clearly there is an additional exothermicity term as  $\nu_c = \frac{1}{N_0 c_p} \frac{\partial Q_c}{\partial T}$  besides the nonlinear ‘ionization-avalanche’ term in the eigenmode now and the system could be stabilized or destabilized depending on the sign of it.

A more detailed stability analysis includes the electron number density [equation (11)] and gas translation temperature [equation (14)]. By including only two equations, electronegative species are excluded ( $n_e \approx n_p$ ) and energy transfer from vibrational energy is negligible (which is reasonable at relatively low gas temperature, see discussions in section 3.2). The characteristic equation is updated to

$$\lambda^2 + \lambda(-\nu_c + \nu_{\text{conv}} + \nu_\beta) + \nu_\beta \nu_{\text{conv}} - \nu_\beta \nu_c - \frac{\partial \hat{\nu}_i}{\partial \left( \frac{\hat{E}}{N} \right)} \nu_J \nu_i = 0 \quad (24)$$

$\nu_\beta$  is defined as electron–ion recombination rate  $\beta_{\text{ep}} n_{e,s}$ . The stability boundary could be written as

$$\nu_c - \nu_{\text{conv}} + \frac{\partial \hat{\nu}_i}{\partial \left( \frac{\hat{E}}{N} \right)} \frac{\nu_J \nu_i}{\nu_\beta} = 0 \quad (25)$$

According to equation (25), the sign of the eigenmodes is determined by the competition among different time scales. A temperature-sensitive reaction heat ( $Q_c \neq 0$ ,  $\frac{\partial Q_c}{\partial T} \neq 0$ ) will not only shift the steady state electron number densities and temperatures, but change the critical current at which  $\text{max}[\text{Re}(\lambda)] = 0$ . The eigenmodes at different current for a

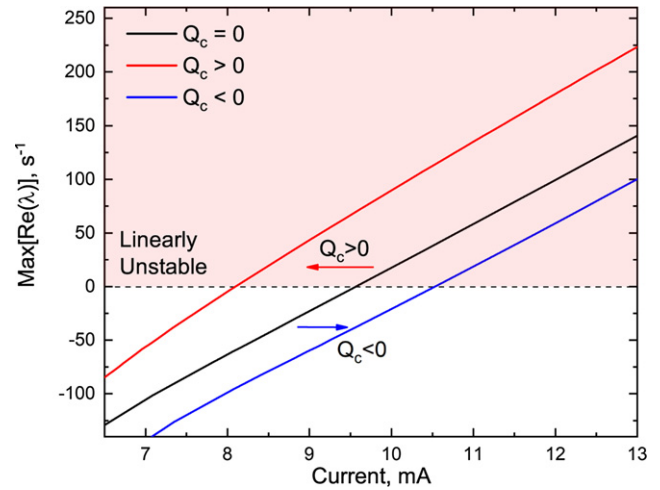


**Figure 2.**  $p = 105$  Torr,  $T_0 = 600$  K.  $Q_c = 0$  refers to a  $\text{N}_2\text{-O}_2$  mixture without any influence from endothermic/exothermic reactions.  $Q_c > 0$  refers to the  $\text{N}_2\text{-O}_2$  mixture with influence from exothermic reactions.  $Q_c < 0$  refers to the  $\text{N}_2\text{-O}_2$  mixture with influence from endothermic reactions.

**Table 1.** The comparison of exothermic and endothermic reactions. Current  $I = 9.5$  mA. The mixture is  $\text{N}_2\text{-O}_2$  at  $T_0 = 600$  K and  $p = 105$  Torr. Convective time scale  $\tau = 1$  ms.  $\tau \frac{\partial Q_c}{\partial T}$  is the chemical heat release/absorption normalized by the heat convection term.  $(\nu_i n_e)^*$  is the normalized ionization term, defined as  $(\nu_i n_e)^* = \frac{\nu_i n_e}{\nu_i n_e(Q_c=0)}$ .

Case	$T_{g,s}$ (K)	$\tau \frac{\partial Q_c}{\partial T}$	$E/N$ (Td)	$(\nu_i n_e)^*$	$\text{max Re}(\lambda)$
$Q_c = 0$	601	0	49.837	1	0
$Q_c > 0$	644	0.33	49.844	1.088	69.4
$Q_c < 0$	537	-0.36	49.827	0.874	-38.0

$\text{N}_2\text{-O}_2$  mixture at 600 K with or without heat release/absorption are calculated, as shown in figure 2. Clearly the original critical current is decreased by an exothermic reaction heat release while increased by an endothermic reaction heat absorption.

To further explore the effect of endothermic/exothermic reactions, a detailed comparison is listed for the three cases at the fixed current shown in table 1. The heat addition or absorption alone will shift the reduced electric field, further modify the ionization term and eventually alter the sign of eigenmodes. By manipulating endothermic/exothermic reactions, the plasma thermal-chemical instability will proceed even at a moderate discharge power input, at which Joule heating is too weak to trigger the classical thermal-ionization mechanism.

The above analysis is performed in the simplified zero-dimensional system. In the realistic reactive plasmas, the  $Q_c$  term may originate from various plasma-assisted chemical reactions. For example, low temperature chemistry in hydrocarbon fuels may provide the heat source of over  $200 \text{ W cm}^{-3}$  at the temperature above 600 K [44, 45]. The exothermic reactions include  $\text{R} + \text{O}_2 \rightleftharpoons \text{RO}_2$  and  $\text{RH} + \text{OH} \rightleftharpoons \text{R} + \text{H}_2\text{O}$ , where RH is the fuel and R is the fuel radical. Chemical kinetics will not merely introduce additional terms in the energy equation. The plasma reaction classes and the species equation will be also updated.

### 3.2. Eigenmodes of different plasma intermediate reaction classes

In molecular plasmas, the thermal-chemical mechanism proceeds through several different plasma reaction classes, which are listed in the mechanism in the supplementary material. Those intermediate plasma reaction classes cut off the direct link between the fluctuation of the electron number density  $\delta n_e$  and the fluctuation of the translational temperature  $\delta T_g$ . One of the most important intermediate plasma reaction classes in the targeted low-electron-energy regime ( $\approx 1$  eV) is the vibrational excitation and the following vibrational–translational (V–T) relaxation.

As the time scale of the vibrational excitation ( $< 10^{-10}$  s) is typically much shorter than that of the V–T relaxation ( $10^{-4}$ – $10^{-2}$  s) [16, 46], the thermal-chemical instability becomes more sensitive to V–T relaxation than to the excitation. To consider the role of V–T relaxation on the stability boundary, equations (11), (14) and (15) are perturbed for the  $N_2$ – $O_2$  mixture. For simplicity, the V–V energy transfer and heat release are ignored ( $\Pi_{VV} = Q_c = Q_c^V = 0$ ). It is assumed there exists only one higher vibrational energy level and the V–T relaxation process in the mixture proceed as  $N_2(v) \rightarrow N_2$ . The characteristic equation for this simplified system is

$$\begin{aligned} & \lambda^3 + \lambda^2(2\nu_{\text{conv}} + \nu_{\beta} + \nu_{\text{VT}}) \\ & + \lambda \left[ \nu_{\beta}\nu_{\text{conv}} + (\nu_{\text{VT}} + \nu_{\text{conv}})(\nu_{\beta} + \nu_{\text{conv}}) - \eta_{\text{T}} \frac{\partial \hat{\nu}_i}{\partial \left(\frac{\hat{E}}{N}\right)} \nu_i \nu_j \right] \\ & + \left[ (\nu_{\text{VT}} + \nu_{\text{conv}}) \left( \nu_{\beta}\nu_{\text{conv}} - \eta_{\text{T}} \frac{\partial \hat{\nu}_i}{\partial \left(\frac{\hat{E}}{N}\right)} \nu_i \nu_j \right) \right. \\ & \left. - \nu_{\text{VT}} \eta_{\text{V}} \frac{\partial \hat{\nu}_i}{\partial \left(\frac{\hat{E}}{N}\right)} \nu_i \nu_j \right] = 0 \end{aligned} \quad (26)$$

where  $\nu_{\text{VT}} = \frac{1}{\tau_{\text{VT}}}$  is the vibrational–translational energy transfer rate. One limit in equation (26) is  $\tau_{\text{VT}} \rightarrow \infty$ , i.e.,  $\nu_{\text{VT}} \rightarrow 0$ . As  $\tau_{\text{VT}}$  is strongly affected by gas temperature, vibrationally-excited species and colliding partners [22, 46],  $\tau_{\text{VT}} \rightarrow \infty$  corresponds to plasmas with the decreasing of the gas temperature and concentrations of chemically-reactive colliding partners. Under such circumstance the energy pumped into the vibrational level is ‘frozen’. Consequently, the critical current is shifted to a larger value to compensate for the energy locked at the vibrational mode. The result is consistent with previous literature [46].

The other limit is the ‘equilibrium’ V–T relaxation process, i.e.  $\tau_{\text{VT}} \rightarrow 0$ , or  $\nu_{\text{VT}} \rightarrow \infty$ . Then equation (26) is simplified into

$$\tau_{\text{VT}} \lambda^3 + \lambda^2 + \lambda(\nu_{\text{conv}} + \nu_{\beta}) + \left( \nu_{\beta}\nu_{\text{conv}} - \frac{\partial \hat{\nu}_i}{\partial \left(\frac{\hat{E}}{N}\right)} \nu_i \nu_j \right) = 0. \quad (27)$$

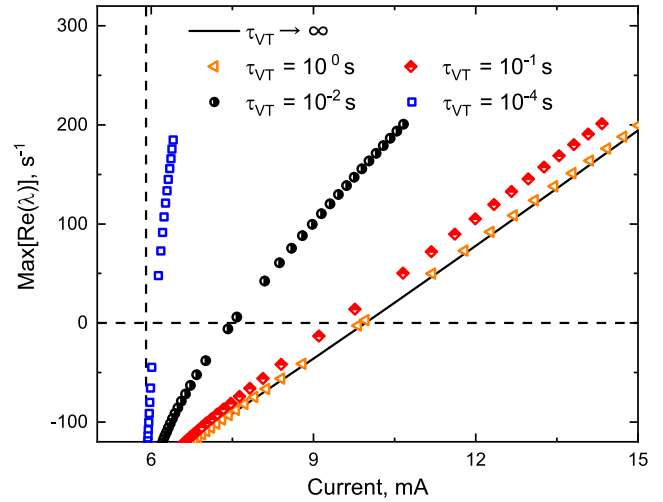


**Figure 3.**  $p = 105$  Torr.  $T_0 = 600$  K. Convective time scale is 1 ms. The maximum eigenvalues at different currents with different vibrational relaxation time scale in the  $N_2$ – $O_2$  mixture.

This is a typical singular perturbation type of equation. As  $\tau_{\text{VT}}$  approaches zero, the energy transfer from the vibrational energy level becomes more dominant. The faster V–T relaxation destabilizes the system more efficiently and the largest eigenmode crosses zero at a smaller current. Between these two limits ( $\tau_{\text{VT}} \rightarrow 0$  and  $\tau_{\text{VT}} \rightarrow \infty$ ), V–T relaxation takes place at a finite rate. Physically, thermal-chemical instability in molecular gases will be slowed down because part of Joule heating is first accumulated in vibrational degrees of freedom of molecules. As temperature perturbation grows,  $\tau_{\text{VT}}$  decreases with temperature and energy stored in the vibrational degree of freedom transforms at an accelerating rate into the translational energy. The above discussions are validated numerically and plotted in figure 3. Certainly, plasma kinetics of vibrationally excited species are much more complicated than the above simplified model. In the detailed  $H_2$ – $O_2$ – $N_2$  mechanism, reactions of vibrationally excited species ( $H_2(v)$ ,  $O_2(v)$  and  $N_2(v)$ ) are considered, including electron-impact vibrational excitation reactions, vibrational–translational (V–T) relaxation reactions, vibrational–vibrational (V–V) exchange reactions, as well as chemical reactions accelerated by vibrationally excited species. The rate constants of V–T reactions are calculated by using the ordinary method of Schwartz, Slawsky and Herzfeld (SSH theory) and some approximations for the Morse oscillator model [47]. For the V–V reactions between two  $H_2(v)$  and  $H_2(v)$  molecules, or  $O_2(v)$  and  $O_2(v)$  molecules, or  $N_2(v)$  and  $N_2(v)$  molecules, the rate constants are calculated by using the equations described in [47]. The chemical reaction rate constants of vibrationally excited species in overcoming the activation energy barrier are calculated by the Fridman–Macheret  $\alpha$ -model [46].

Another key intermediate plasma reaction class in the molecular gas discharge is the electron attachment and detachment reactions. The charged particle distribution in the contracted state with different attachment rates has been discussed

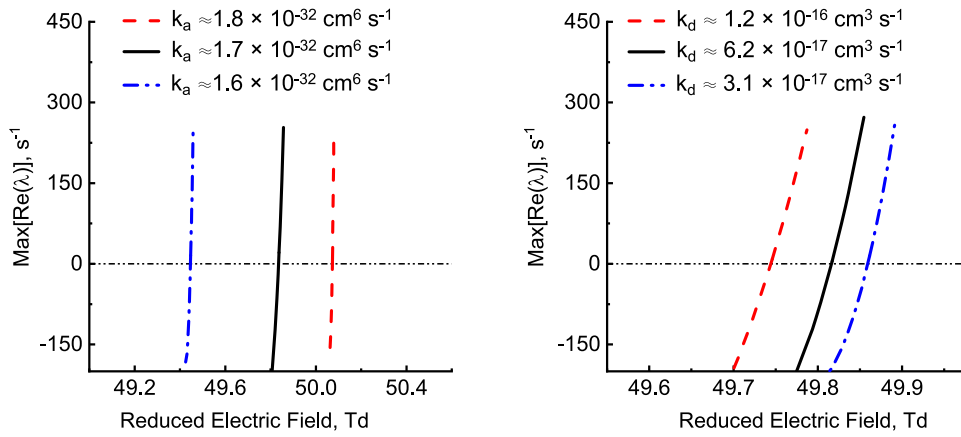


**Figure 4.**  $p = 70$  Torr.  $T_0 = 400$  K. Convective time scale is 1 ms. Left: the maximum eigenvalues at different  $E/N$  with different three-body attachment coefficients in  $N_2$ – $O_2$  mixture. Right: the maximum eigenvalues at different  $E/N$  with different detachment coefficients in  $N_2$ – $O_2$  mixture.

in our previous paper [23]. The impact of electron attachment/detachment reactions on the stability boundary will be analyzed here.

A perturbation of equation (12) at the steady state (i.e.,  $dn_n/dt = 0$ ) yields

$$\delta n_n = \frac{\bar{\nu}_a - \bar{\beta}_{ii} n_n}{1/\tau + \bar{\nu}_d + \bar{\beta}_{ii} n_e + 2\bar{\beta}_{ii} n_n} \delta n_e. \quad (28)$$

From equation (28), when the system is departed from a steady state, different attachment/detachment rates will affect the balance between electrons and negative ions, and implicitly shift the linear stability of the system. Figure 4 shows the maximum magnitudes of the eigenmodes under different attachment/detachment rates calculated from a simplified  $N_2$ – $O_2$  system. Stronger electron attachment accelerates the conversion from electrons to ions, making the electron number density, mobility and further Joule heating lower. The stabilization effect shifts the critical reduced electric field ( $E/N$ ) to a larger value. In other words, a larger ionization term  $\nu_i(E/N)$  is required for the system to cross the stability boundary. On the contrary, stronger detachment leads to higher electron productions. Extra electrons destabilize the system even when  $E/N$  is at a smaller value and ionization rates are at lower levels.

The above discussed V–T relaxation and electron attachment/detachment reactions are representative classes of the intermediate plasma reactions. The analysis is based on the simplified system, but it is helpful for the understanding of the stability in the multi-component chemical system introduced in section 3.3, where elementary kinetics lead to a large variation in the composition and temperature. More complicated vibrational reactions are considered and the mixture-averaged attachment/detachment rates vary dramatically with the progress of the kinetics.

### 3.3. TCMA of elementary kinetics

The analytical stability criterion provides insights of how exothermic/endothermic reactions or specific reaction classes such as V–T relaxation or electron attachment/detachment will influence the stability boundary. They are some important

**Table 2.** Detailed setup of three cases for the demonstration of the impact of elementary kinetics on the thermal-chemical mechanism.

Case	$T_0$ (K)	$p$ (Torr)	$I$ (mA)	$\tau$ (ms)	Initial gas composition
I	800	200	0.5	5	$N_2:O_2 = 80:20$
II	800	200	0.5	5	$N_2:O_2:H_2 = 80:6.7:13.3$
III	825	200	0	5	$N_2:O_2:H_2 = 80:6.7:13.3$

facets of the thermal-chemical mechanism for the contraction of the plasma volume. However, to further discuss the general effects from chemistry, one has to resort to the detailed chemical kinetic formulation in section (2.1), perform numerical perturbative analysis and reveal chemical modes of a large chemical system with various species and reactions.

In this work, three test cases are compared to demonstrate impact of kinetic coupling between  $H_2$ – $O_2$ – $N_2$  ignition chemistry and plasma contraction chemistry on the TCMs [defined in equation (20)] in a plasma-assisted ignition process. The setup of three cases is summarized in table 2. Case I is the normal plasma thermal-ionization instability in air with a limited current input. Case II is the plasma thermal-chemical instability in a stoichiometric  $N_2$ – $O_2$ – $H_2$  mixture under the same current. Case III is the homogeneous ignition using the same initial chemical composition as case II. The initial temperature is adjusted purposely from 800 K to 825 K in case III to increase the system reactivity and to make the chemical time scale close to each other [ $\sim \mathcal{O}(10$  ms)] for all three cases.

The time-dependent profiles of positive TCMs, temperatures, major species, and electron production/consumption reactions are plotted in figure 5. The first column is the results of case I [figures 5(a), (d) and (g)], under a limited current input ( $I = 0.5$  mA) and strong convection ( $\nu_{conv} = 1/\tau = 2 \times 10^2$  s $^{-1}$ ). The system temperature increases slowly by Joule heating and all positive TCMs are suppressed (all below 10 s $^{-1}$ ). The reduced electric field is around 40 Td and the electron energy is around 0.75 eV, at which a considerable fraction of energy is pumped into vibrational levels of  $N_2$  and  $O_2$  via electron-impact excitation reactions. Vibrational excited species further transfer energy among different vibrational

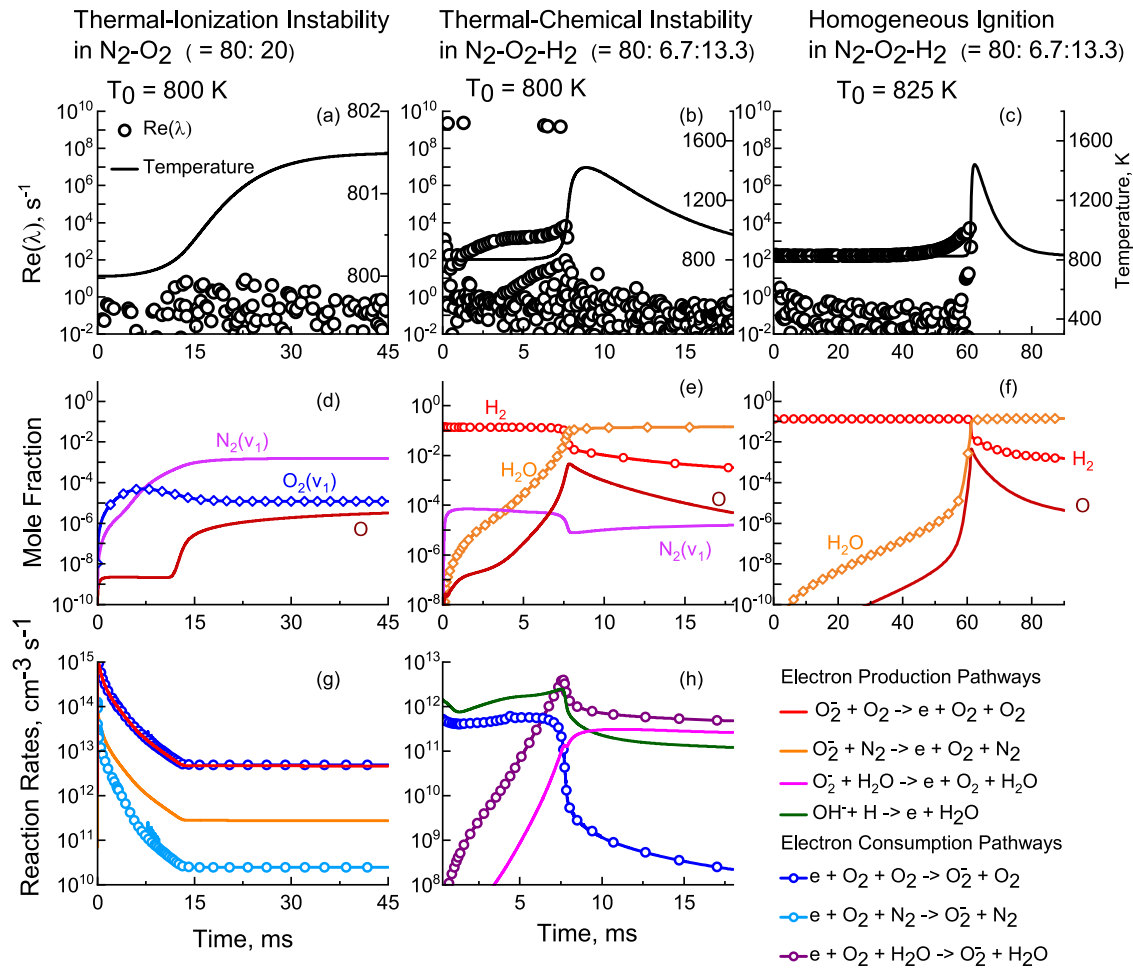
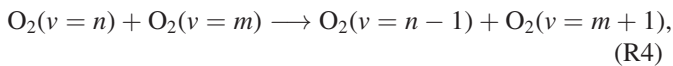
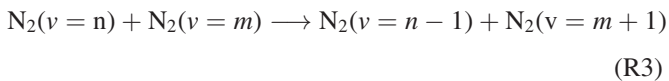
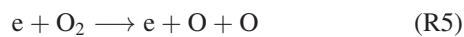


**Figure 5.** Comparisons among three cases [thermal-ionization instability: (a, d, g), thermal-chemical instability: (b, e, h), homogeneous ignition (c, f)] for the discussion of elementary kinetics. All x-axes for (a)–(h) are time in millisecond. Left y-axes for (a)–(c) are eigenvalues  $\text{Re}(\lambda)$  in  $\text{s}^{-1}$ . Only positive eigenvalues (explosive TCMs) are plotted in the logarithmic scale. Right y-axes for (a)–(c) are temperature in K. Y-axes for (d)–(f) are mole fractions for active species. Y-axes for (g)–(h) are reaction rates of major reactions for the electron production and consumption (in molecule  $\text{cm}^{-3} \text{s}^{-1}$ ). Pressure  $p = 200$  Torr. Convective time scale  $\tau = 5$  ms. The current for simulating plasma instabilities are  $I = 0.5$  mA.

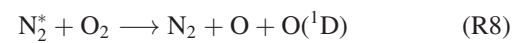
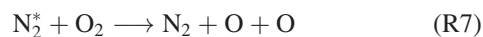
levels via the V–V energy exchange such as



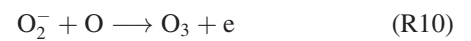
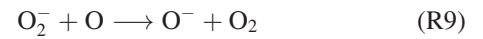
where  $m$  and  $n$  indicate the vibrational levels, which are 1–8 for  $\text{N}_2(v)$  and 1–4 for  $\text{O}_2(v)$  considered in this study. Reactive radicals such as the atomic oxygen have low number density and are generated either via the electron-impact dissociation reactions such as



or collisional dissociation by electronically excited nitrogen (denoted as  $\text{N}_2^*$ ) as



Atomic oxygen is consumed via ion conversion reactions such as



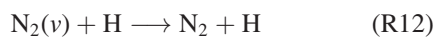
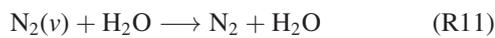
The electron production/consumption pathways in this case are mainly the three-body detachment/attachment reactions from negative oxygen ions  $\text{O}_2^-$  [shown in figure 5(g)], consistent with the previous studies [20, 21, 23]. Results from case III are plotted in figures 5(c) and (f). The homogeneous ignition in the  $\text{H}_2$ – $\text{O}_2$ – $\text{N}_2$  system occurs at approximately 60 ms with the leading positive eigenmodes increasing from  $\mathcal{O}(10^2 \text{ s}^{-1})$  to  $\mathcal{O}(10^3 \text{ s}^{-1})$ . After the ignition, positive TCMs decay dramatically as the convective heat loss lowers the reactivity and the system converges to the chemical equilibrium.

The distinctive feature of the plasma thermal-chemical instability is the coupling between plasma kinetics and

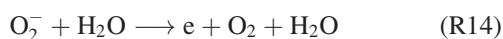
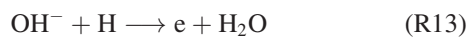
**Table 3.** The list of time ( $t$ , unit: ms), largest positive eigenmodes ( $\text{Re}(\lambda)$ , unit:  $\text{s}^{-1}$ ), the corresponding RAS, and the temperature ( $T$ , unit: K) for all three cases.

Case I				Case II				Case III			
$t$	$\text{Re}(\lambda)$	RAS	$T$	$t$	$\text{Re}(\lambda)$	RAS	$T$	$t$	$\text{Re}(\lambda)$	RAS	$T$
6	$1.4 \times 10^{-2}$	NO <sub>2</sub>	800	0.5	$2.3 \times 10^9$	N <sub>2</sub> ( $v = 6$ )	800	6	$1.6 \times 10^2$	O	825
7	$1.7 \times 10^{-1}$	NO	800	1	$1.1 \times 10^1$	O	800	7	$1.6 \times 10^2$	OH	825
8	$1.6 \times 10^{-1}$	N <sub>2</sub> O	800	2	$4.8 \times 10^2$	N <sub>2</sub> ( $v = 8$ )	801	16	$1.6 \times 10^2$	HO <sub>2</sub>	825
9	$1.4 \times 10^{-1}$	O	800	3	$1.1 \times 10^3$	N <sub>2</sub> ( $v = 5$ )	801	17	$1.6 \times 10^2$	OH	825
16	$3.6 \times 10^0$	NO	800	5	$1.6 \times 10^3$	O <sub>2</sub> ( $v = 2$ )	803	58	$1.8 \times 10^3$	OH	825
17	$2.1 \times 10^0$	N	800	6	$1.8 \times 10^3$	H <sub>2</sub> ( $v = 1$ )	810	59	$2.4 \times 10^3$	O	826
18	$1.7 \times 10^0$	N <sub>2</sub> (A)	800	7	$3.2 \times 10^3$	H <sub>2</sub> ( $v = 3$ )	845	60	$2.8 \times 10^3$	O	834
19	$1.6 \times 10^0$	NO	800	7.5	$6.5 \times 10^3$	N <sub>2</sub> O	1000	61	$6.3 \times 10^3$	HO <sub>2</sub>	993
19.5	$1.3 \times 10^0$	N <sub>2</sub> (A)	800	8	$4.4 \times 10^1$	H <sub>2</sub> O <sub>2</sub>	1328	61.2	$1.2 \times 10^3$	H <sub>2</sub>	1190
20	$1.1 \times 10^0$	N	800	9	$5.1 \times 10^{-1}$	H <sub>2</sub> O	1420	63	$1.3 \times 10^{-3}$	O	1422
27	$5.1 \times 10^0$	O	801	15	$8.7 \times 10^{-1}$	O <sub>2</sub>	1080	70	$1.2 \times 10^{-3}$	O <sub>2</sub>	1025
28	$1.9 \times 10^0$	N	801	20	$1.2 \times 10^{-1}$	N <sub>2</sub>	920	75	$1.2 \times 10^{-3}$	H	918

combustion kinetics [plotted in figures 5(b), (e) and (h)]. The Joule heating from the discharge provides the initial energy to increase the temperature and ‘activates’ unstable TCMs of the H<sub>2</sub>–O<sub>2</sub>–N<sub>2</sub> mixture. In figure 5(b), there is a clear growth trend for the magnitude of the TCMs in the initial 7 ms, ranging from  $\mathcal{O}(10^0 \text{ s}^{-1})$  to  $\mathcal{O}(10^4 \text{ s}^{-1})$ . This is due to the active energy relaxation from vibrational energies of the excited major species (H<sub>2</sub>, N<sub>2</sub>, and O<sub>2</sub>) to neutral species. Meanwhile, the excited species generated from plasma kinetics interact with each other through reactions like V–V energy exchange and combustion kinetics of the H<sub>2</sub>–O<sub>2</sub>–N<sub>2</sub> chemistry, contributing greatly to the gas heating and enhancing the transition from the homogeneous state to the contracted state. At approximately 7 ms, the plasma-assisted ignition occurs with a sharp temperature rise over 400 K and the magnitude of TCMs increases promptly. In addition, new reaction pathways for plasma species are created with the progress of the H<sub>2</sub>–O<sub>2</sub>–N<sub>2</sub> chemistry. For example, vibrationally excited nitrogen N<sub>2</sub>( $v$ ) is deactivated by H radicals and H<sub>2</sub>O produced during the ignition process as



New kinetic pathways are also established for the creation of electrons as

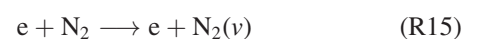


Moreover, although the consumption of electrons is still governed by three-body attachment to oxygen and the formation of oxygen ions, the major collision partners are now switched from N<sub>2</sub> and O<sub>2</sub> in the air case to H<sub>2</sub>O in the plasma-assisted ignition case.

From the above analysis, the time-dependent explosive chemical modes differ greatly in the normal thermal-ionization instability (case I) and the thermal-chemical instability (case II) even at the same discharge current input. Chemical kinetics provide new unstable modes to the system. To further understand how TCMs are related to different species, the time-dependent species/temperature pointer (SP) following equation (21) are computed and the RAS for the corresponding eigenmodes are listed in table 3.

In case I, most RAS are related with N<sub>2</sub>–O<sub>2</sub> chemistry and NO<sub>x</sub> formation. Those NO<sub>x</sub> species including NO<sub>2</sub>, NO and N<sub>2</sub>O are in low number densities (below  $10^6 \text{ cm}^{-3}$ ) and the corresponding positive TCMs are suppressed to small values. Chemical modes related with excited species like N<sub>2</sub>(A) may dominate from time to time. However, their growth rate is too small to trigger the exponential transition from homogeneous state to the unstable state. In other words, all of the unstable modes are not fully activated and the system only goes through a moderate change. In case III, RAS is consistent with previous studies of H<sub>2</sub>–O<sub>2</sub> chemistry [29]. Small radicals including OH, H and O dominate the unstable ignition progress and no excited species are representing or leading the explosive TCMs. In this case only unstable modes from H<sub>2</sub>–O<sub>2</sub> chemistry are fully activated.

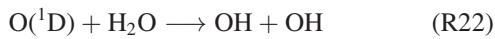
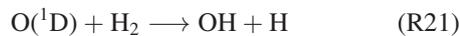
Eigenmodes and their RAS are quite different in case II. Before the plasma assisted ignition and dramatic changes in rates of H<sub>2</sub>–O<sub>2</sub> elementary reactions and heat release, TCMs related with small radicals such as O contribute to the destabilization of the plasma system, similar as those in case III. Moreover, excited species generated from extremely fast plasma kinetics also have significant impact on the unstable modes of the system. For example, vibrationally and electronically excited nitrogen are produced from electron-impact reactions as



The excited species produced in plasma will further provide reactive radicals to the radical pool to enhance ignition via



The typical concentrations of vibrationally excited species are covering a wide range in magnitudes, from  $\mathcal{O}(10^{12} \text{ cm}^{-3})$ – $\mathcal{O}(10^{14} \text{ cm}^{-3})$  for low vibrational levels to  $\mathcal{O}(10^6 \text{ cm}^{-3})$ – $\mathcal{O}(10^8 \text{ cm}^{-3})$  for high vibrational levels. As a result, the magnitudes of the TCMs led by vibrationally excited species can be as large as  $\mathcal{O}(10^9 \text{ s}^{-1})$ . For electronically excited species such as  $\text{N}_2(\text{C})$  and  $\text{N}_2(\text{a}')$ , even though the typical concentration is below  $\mathcal{O}(10^8 \text{ cm}^{-3})$ , the fast quenching relaxation reactions shown above (R19) and (R20) with reaction rates over  $\mathcal{O}(10^{12} \text{ cm}^{-3} \text{ s}^{-1})$  will generate TCMs with growth rates of over  $10^4 \text{ s}^{-1}$ . At the time of ignition, excited species including  $\text{O}(\text{}^1\text{D})$  and  $\text{N}_2(v)$  continue to accelerate the reaction progress and lead the unstable TCMs via the aforementioned vibrational-translational excitation and  $\text{O}(\text{}^1\text{D})$  reactions as

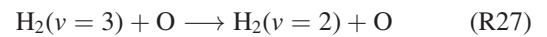
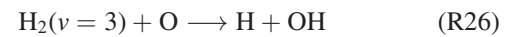


In this case, TCMs reveal a strong coupling between  $\text{H}_2$ – $\text{O}_2$  ignition chemistry, represented by small radicals such as OH or  $\text{HO}_2$  with the plasma chemical kinetics, represented by the reactions involving electrons and excited species. What's more, TCMA shows that plasma-generated active species such as N or NNH (related with  $\text{N}_2$ – $\text{H}_2$  kinetics), and NO or  $\text{N}_2\text{O}$  (related with  $\text{N}_2$ – $\text{O}_2$  kinetics) are involved in the explosive modes as they participate in the energy relaxation process of vibrationally or electronically excited species as



Those fully-activated unstable modes generalize the original thermal-ionization instability to thermal-chemical instability. Figure 6 visualizes some representative TCMs and the associated major species identified by the SP [defined in equation (21)]. Before the ignition [shown in figure 6(a)], TCMs with large positive eigenvalues are mostly dominated by

vibrationally excited species. The discharge-deposited energy transfers via electrons and different vibrational levels of different species, leading to radical formation and temperature rise. Conventional  $\text{H}_2$ – $\text{O}_2$  combustion modes are still present [as 'mode 3' in figure 6(a)], but based on its eigenvalue, this mode with such a small growth rate can hardly trigger the ignition nor the instability in the millisecond time scale alone. Upon the ignition [shown in figure 6(b)], TCMA allows for a clear separation of different modes and provides an overview for reaction dynamics and active species in the thermal-chemical instability. For this case, the dominant mode is still governed by vibrationally-excited plasma-combustion chemistry as  $\text{H}_2(v)$  goes through the chain-branching and energy relaxation reactions as



The second and third largest modes at  $t = 7 \times 10^{-3} \text{ s}$  correspond to the coupling between  $\text{H}_2$ – $\text{O}_2$  chemistry and electronically-excited plasma kinetics. Conventional  $\text{H} + \text{OH}(+\text{M}) \rightarrow \text{H}_2\text{O}(+\text{M})$  (M is a third body) still proceeds and the energy relaxation from less-populated electronically excited species still contributes to the dynamics and chemical modes of the system.

In summary, unstable TCMs with multiple time-scales coexist when the thermal-chemical instability is triggered in the presence of elementary kinetics. Plasma kinetics at the sub-millisecond scales boost and couple with the  $\text{H}_2$ – $\text{O}_2$ – $\text{N}_2$  kinetics and thus the electron production/consumption pathways are modified greatly. Various excited species are actively involved and interacted in the transition process of the plasma thermal-chemical instability. A systematic method, TCMA, is able to decompose and identify individual TCMs and provides insights of the elementary kinetics of the instability. Future experimental studies are also required to further validate the effect from elementary kinetics on the plasma thermal-chemical instability.

#### 3.4. Stability criterion in the voltage–current characteristic curve

Negative differential conductivity (NDC) in the voltage–current characteristic curve is a major feature of the thermal-ionization mechanism [48–50]. Previous multi-dimensional simulations [20, 21, 23, 50] already show that there exists a hysteresis transition. In the bistable region shown in figure 7(a), the homogeneous plasma discharge will transit into a contracted state by a strong enough perturbation. With the inclusion of chemical kinetics, how the steady-state voltage–current curve will evolve is analyzed in the following content. Due to the limit of zero-dimensional modeling, the focus is the homogeneous ['upper' in figure 7(a)] branch with a high electric field and low electron number density. The contribution from the diffusion in the transition is beyond the scope of this work.

First it is shown that in the non-reactive case the stability boundary in the homogeneous branch has a distinctive

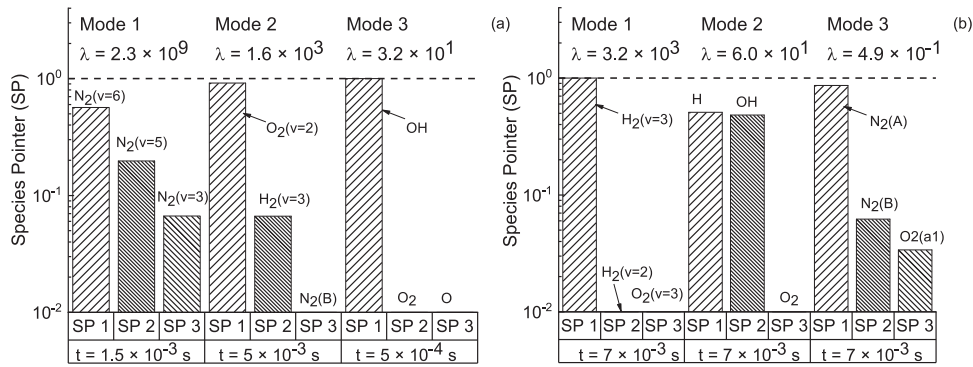


**Figure 6.** (a) The distributions of SP for three TCMs before the plasma assisted ignition of  $H_2$ – $O_2$ – $N_2$  system. They are selected from  $t = 1.5 \times 10^{-4}$  s,  $5 \times 10^{-3}$  s and  $5 \times 10^{-4}$  s without the loss of generality. For every mode, top three species with their SP values [defined in equation (21)] are visualized. (b) The distributions of SP for three TCMs at the plasma assisted ignition event of  $H_2$ – $O_2$ – $N_2$  system. The modes are selected from the same time  $t = 7 \times 10^{-3}$  s, at which the temperature of the system is 845 K. For both (a) and (b), selected modes are displayed in a descending order of the eigenvalues.

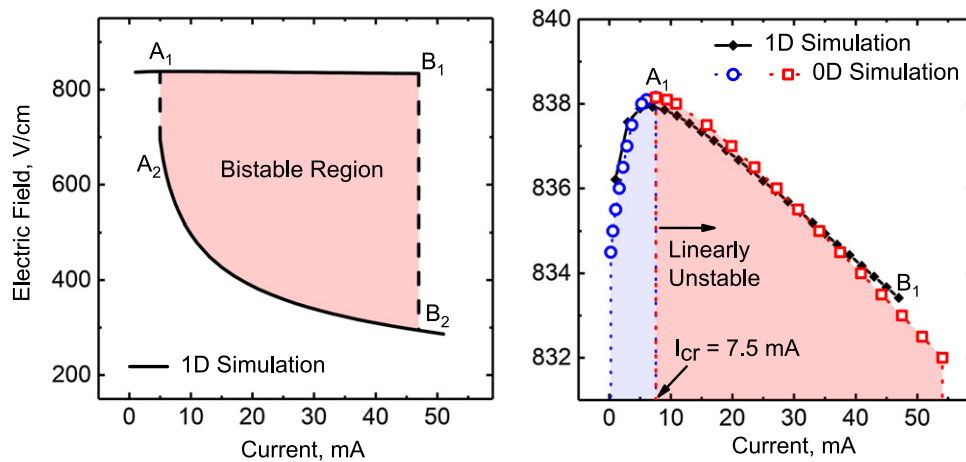


**Figure 7.** Left: current–voltage characteristics using the one-dimensional simulation in a  $N_2$ – $O_2$  mixture. The simulation has been reported in [23, 24].  $p = 70$  Torr and  $T_0 = 400$  K. Convective time scale  $\tau = 1$  ms. Right: the comparison of the homogeneous branch of the current–voltage characteristics using zero-dimensional and one-dimensional simulation under the same condition. The linearly stable (in blue) and unstable (in red) region are separated by the stability boundary. The critical current in this case is 7.5 mA.

geometrical feature: the bifurcation point as  $\max[\text{Re}(\lambda)] = 0$  happens to be the extreme point of the curve  $E = E(I)$ , i.e.  $dE/dI = 0$ . Start from equation (9),  $dE/dI$  is expressed as

$$\frac{dE}{dI} = \frac{dE/d\sigma}{S(\sigma + E dE/d\sigma)} \quad (29)$$

For every steady state,  $[dE/d\sigma]_s$  can be derived simply by equating the rhs of equations (11)–(15) to zero. In the simplest case, by considering electro-positive species (negative ion is negligible) without vibrational–translational energy transfer and heat addition ( $\nu_c = 0$ ), then  $[dE/d\sigma]_s = 0$  is equivalent to

$$\frac{\partial \hat{\nu}_i}{\partial \left(\frac{E}{N}\right)} \nu_{1i} \nu_i - \nu_{\beta} \nu_{\text{conv}} = 0 \quad (30)$$

which is exactly the condition when  $\lambda = 0$  in the characteristic equation as equation (24). In other words,

$$dE/dI = 0 \Leftrightarrow \max[\text{Re}(\lambda)] = 0 \quad (31)$$

This relation could be extended to the case where attachment, vibrational relaxation and heat addition are considered. A validation result of equation (31) is shown in figure 7. The bifurcation point  $A_1$  separates the homogeneous branch into linearly stable and unstable part. This figure also demonstrates the consistency between 0D modeling assumption used in this work and the 1D modeling result reported in our previous paper for small currents. With the increase of the current, in the 1D modeling, a sudden jump occurs at point  $B_1$  and physically represents the transition from the homogeneous state to a contracted state (point  $B_2$ ). In the 0D modeling, the electric field also keeps dropping with the increase of the current. However, without ambipolar diffusion and other physical mechanisms, discrepancies appear between those two modeling approaches at larger currents. Future stability analysis in a multi-dimensional modeling framework is still required to further reveal how spatial inhomogeneity will be coupled with unstable thermal-chemical modes.

In the presence of chemical kinetics, the characteristic curve  $E = E(I)$  or the slope as  $dE/dI$  or  $dE/d\sigma$  will be reshaped

by species and reactions. Consider the fully perturbed form of equations (11)–(15) and make several algebraic manipulations (details are revealed in the supplementary material), one can reach the following result as

$$\left[ \frac{\delta(\ln \sigma)}{\delta(\ln E)} \right]^{-1} = \left[ \frac{1}{\Delta' / \delta(\ln n_e) |\delta(\ln E)|} + \frac{\sum \nu_{i,j} \delta x_j}{\sum x_j \nu_{i,j} \nu'_{i,j} |\delta(\ln E)|} - 1 \right] \times \frac{\delta C - \delta V - \sum \frac{\partial h_j}{\partial T} \omega_j T - \sum h_j \frac{\partial \omega_j}{\partial T} T}{\eta_T \sigma E_s^2} - 2 \quad (32)$$

where  $\Delta'$  represents interactions between ionization and other plasma kinetics (see supplementary material for more details) and scales linearly with the normalized ionization sensitivity  $\nu'_{i,j}$  for species  $j$ , defined as

$$\nu_{i,j}' = \left[ \frac{\partial \nu_{i,j}}{\partial (E/N)} \right]_s / \left[ \frac{\nu_{i,j}}{(E/N)} \right]_s \quad (33)$$

In other words,  $\Delta'$  is larger with a larger normalized ionization sensitivity of species  $j$ .  $\nu_{i,j}$  is the ionization rate of individual species  $j$ .  $\delta x_j$  represents the change of the mass fraction for species  $j$ .  $\delta C$  and  $\delta V$  are the cooling term and the energy release term from vibrational relaxation.  $\partial h_j / \partial T$  represents the change of the enthalpy for species  $j$  with respect to temperature while  $\partial \omega_j / \partial T$  represents the change of the total reaction rates for species  $j$  with respect to temperature. Equation (32) clearly encodes the original thermal-ionization mechanism. Joule heating ( $\eta_T \sigma E_s^2$ ), ionization and other plasma kinetics ( $\Delta'$ ) will influence the differential conductivity. More importantly, chemical kinetics are shown to change the sign of  $dE/dI$  and drive the system into the NDC region ( $dE/dI < 0$ ). The composition update of the mixture ( $\sum \nu_{i,j} \delta x_j$ ), the change of specific heat for individual species  $j$  as  $\partial h_j / \partial T$  (consistent with previous discussions of ‘ $c_p$ -controlled plasma’ [25, 26]), the change of reaction rates ( $\partial \omega_j / \partial T$ ) will all contribute to modifying differential conductivity from positive values to negative values.

Physically, when the system is under the NDC region, the filament with a higher local current has a lower electric field. Any departure from the steady states, such as a fluctuation of field, will tend to grow rather than dissipate. Equation (32) clearly shows that NDC is also influenced by different chemical kinetics. The characteristic curve is expected to change dramatically by the thermal-chemical mechanism compared to the classical  $E = E(I)$  curve governed only by the thermal-ionization mechanism (shown in figure 7).

#### 4. Conclusion

A general model together with an analytical criterion of plasma thermal-chemical instability is presented for a zero-dimensional plasma system. The eigenmodes of the thermal-chemical instability involving different plasma energy transfer processes and chemical reaction classes such as

vibrational–translational (V–T) relaxation, electron attachment/detachment, and elementary combustion kinetics are investigated. It is shown that the stability criterion or the critical discharge parameter are significantly modified by plasma enhanced reaction kinetics. The TCMA with detailed kinetics is performed in a  $H_2$ – $O_2$ – $N_2$  system. It is shown that the explosive mode species/temperature pointer (SP) can successfully identify the important species, defined as ‘RAS’, and their associated elementary reactions, which contribute greatly to the onset of the instability. The RAS of chemical modes of plasma thermal-chemical instability differ greatly from the plasma thermal instability and the normal homogeneous ignition. Kinetic pathways including fuel oxidation by vibrational and electronically excited species are shown to be important during the initiation of the ‘explosion’ of the thermal-chemical modes in the system. Plasma instability and chemical kinetics interact in a variety of time-scales from millisecond to sub-microsecond. Moreover, the characteristic current–voltage curve is also reshaped by chemical kinetics. Therefore, understanding the impact of chemical kinetics on plasma instability will provide more insights for the control of plasma instability for various applications from efficient ignition to material synthesis.

#### Acknowledgments

This work was supported by NSF grant on plasma instability (NSF CBET-1903362), NSF grant on chemical manufacturing (NSF EFRI DChEM-2029425), DOE grant of Plasma Science Center (DE-SC0020233) and DOE NETL grant (DE-FE0026825). HZ is grateful for support from Eli and Britt Harari Fellowship at Princeton University. HZ also acknowledges the valuable opportunity to discuss CSP with Professor Sau-Hai (Harvey) Lam, a role model, an outstanding mathematician and the founder of CSP theory. The authors also thank Timothy Chen, Tianhan Zhang, Dr. Aric Rouso and Dr. Shuqun Wu at Princeton University for helpful discussions.

#### ORCID iDs

Hongtao Zhong  <https://orcid.org/0000-0003-4064-6298>  
 Mikhail N Shneider  <https://orcid.org/0000-0002-2925-7008>  
 Xingqian Mao  <https://orcid.org/0000-0003-1042-5144>

#### References

- [1] Smith K and Thomson R M 1978 *Computer Modeling of Gas Lasers* (Berlin: Springer)
- [2] Nighan W L, Wiegand W J and Haas R A 1973 Ionization instability in  $CO_2$  laser discharges *Appl. Phys. Lett.* **22** 579–82
- [3] Nighan W L and Wiegand W J 1974 Causes of arcing in cw  $CO_2$  convection laser discharges *Appl. Phys. Lett.* **25** 633–6
- [4] Jacob J H and Mani S A 1975 Thermal instability in high-power laser discharges *Appl. Phys. Lett.* **26** 53–5
- [5] Raizer Y P, Milikh G M and Shneider M N 2006 On the mechanism of blue jet formation and propagation *Geophys. Res. Lett.* **33** L23801

- [6] Milikh G M, Shneider M N and Mokrov M S 2014 Model of blue jet formation and propagation in the nonuniform atmosphere *J. Geophys. Res. Space Phys.* **119** 5821–9
- [7] Starikovskiy A and Aleksandrov N 2013 Plasma-assisted ignition and combustion *Prog. Energy Combust. Sci.* **39** 61–110
- [8] Adamovich I V and Lempert W R 2014 Challenges in understanding and predictive model development of plasma-assisted combustion *Plasma Phys. Control. Fusion* **57** 014001
- [9] Popov N A 2016 Kinetics of plasma-assisted combustion: effect of non-equilibrium excitation on the ignition and oxidation of combustible mixtures *Plasma Sources Sci. Technol.* **25** 043002
- [10] Engelhardt M, Ries S, Hermanns P, Bibinov N and Awakowicz P 2017 Modifications of aluminum film caused by micro-plasmas and plasma spots in the effluent of an argon non-equilibrium plasma jet *J. Phys. D: Appl. Phys.* **50** 375201
- [11] Whitehead J C 2016 Plasma-catalysis: the known knowns, the known unknowns and the unknown unknowns *J. Phys. D: Appl. Phys.* **49** 243001
- [12] Sobiecki J R, Wierzchon T, Karpinski T and Rudnicki J 2000 Modification of the microstructure and properties of Ti–1Al–1Mn titanium alloy due to nitriding and oxynitriding under glow discharge conditions *Fourth Institute of Materials Int. Conf. on the Microstructure of High Temperature Materials: Microstructure and Properties of Titanium Alloys* pp 229–35
- [13] Choi I, Uddi M, Jiang N, Adamovich I and Lempert W 2009 Stability and heating rate of air and ethylene-air plasmas sustained by repetitive nanosecond pulses *47th AIAA Aerospace Sciences Meeting* p 688
- [14] Kerner B S and Osipov V V 1989 *Sov. Phys. Usp.* **32** 101
- [15] Ecker G, Kroß W and Zoßler O 1964 Thermal instability of the plasma column *Phys. Fluids* **7** 2001–6
- [16] Haas R A 1973 Plasma stability of electric discharges in molecular gases *Phys. Rev. A* **8** 1017
- [17] Allis W P 1976 Review of glow discharge instabilities *Physica B* **82** 43–51
- [18] Velikhov E P, Golubev V S and Pashkin S V 1982 Glow discharge in a gas flow *Sov. Phys. Usp.* **25** 340
- [19] Golubovskii Y B, Nekuchaev V, Gorchakov S and Uhrlandt D 2011 Contraction of the positive column of discharges in noble gases *Plasma Sources Sci. Technol.* **20** 053002
- [20] Shneider M N, Mokrov M S and Milikh G M 2012 Dynamic contraction of the positive column of a self-sustained glow discharge in molecular gas *Phys. Plasmas* **19** 033512
- [21] Shneider M N, Mokrov M S and Milikh G M 2014 Dynamic contraction of the positive column of a self-sustained glow discharge in air flow *Phys. Plasmas* **21** 032122
- [22] Raizer Y P 1991 *Gas Discharge Physics* (Berlin: Springer)
- [23] Zhong H, Shneider M N, Mokrov M S and Ju Y 2019 Thermal-chemical instability of weakly ionized plasma in a reactive flow *J. Phys. D: Appl. Phys.* **52** 484001
- [24] Zhong H, Shneider M N, Mokrov M S and Ju Y 2020 Thermal-chemical plasma instability in a reacting flow *AIAA Scitech 2020 Forum* p 1661
- [25] Wolf A J, Righart T W H, Peeters F J J, Bongers W A and van de Sanden M C M 2020 Implications of thermo-chemical instability on the contracted modes in CO<sub>2</sub> microwave plasmas *Plasma Sources Sci. Technol.* **29** 025005
- [26] Viegas P, Vialetto L, Wolf A J, Peeters F, Groen P W, Righart T H, Bongers W, Van de Sanden R and Diomede P 2020 Insight into contraction dynamics of microwave plasmas for CO<sub>2</sub> conversion from plasma chemistry modelling *Plasma Sources Sci. Technol.* **29** 105014
- [27] Rousso A C, Goldberg B M, Chen T Y, Wu S, Dogariu A, Miles R B, Kolemen E and Ju Y 2020 Time and space resolved diagnostics for plasma thermal-chemical instability of fuel oxidation in nanosecond plasma discharges *Plasma Sources Sci. Technol.* **29** 105012
- [28] Golubovskii Y, Valin S, Pelyukhova E and Nekuchaev V 2019 Instabilities of a constricted gas discharge with respect to two-dimensional wave perturbations *Plasma Sources Sci. Technol.* **28** 045015
- [29] Lam S H and Goussis D A 1989 Understanding complex chemical kinetics with computational singular perturbation *Symp. (Int.) on Combustion* (Elsevier) 22 931–41
- [30] Lu T F, Yoo C S, Chen J H and Law C K 2010 Three-dimensional direct numerical simulation of a turbulent lifted hydrogen jet flame in heated coflow: a chemical explosive mode analysis *J. Fluid Mech.* **652** 45
- [31] Douglas-Hamilton D H and Mani S A 1973 An electron attachment plasma instability *Appl. Phys. Lett.* **23** 508–10
- [32] Flitti A and Pancheshnyi S 2009 Gas heating in fast pulsed discharges in N<sub>2</sub>–O<sub>2</sub> mixtures *Eur. Phys. J. Appl. Phys.* **45** 21001
- [33] Mao X, Chen Q, Rousso A C, Chen T Y and Ju Y 2019 Effects of controlled non-equilibrium excitation on H<sub>2</sub>/O<sub>2</sub>/He ignition using a hybrid repetitive nanosecond and DC discharge *Combust. Flame* **206** 522–35
- [34] Pancheshnyi S, Eismann B, Hagelaar G J M and Pitchford L C 2008 *Computer Code Zdplaskin* (Toulouse, France: University of Toulouse, LAPLACE, CNRS-UPS-INP)
- [35] Lutz A E, Kee R J and Senkin J A M 1988 A fortran program for predicting homogeneous gas phase chemical kinetics with sensitivity analysis *Technical Report* (Livermore, CA USA: Sandia National Labs)
- [36] Mao X, Rousso A, Chen Q and Ju Y 2019 Numerical modeling of ignition enhancement of CH<sub>4</sub>/O<sub>2</sub>/He mixtures using a hybrid repetitive nanosecond and dc discharge *Proc. Combust. Inst.* **37** 5545–52
- [37] Zhong H, Mao X, Rousso A C, Patrick C L, Yan C, Xu W, Chen Q, Wysocki G and Ju Y 2020 Kinetic study of plasma-assisted n-dodecane/O<sub>2</sub>/N<sub>2</sub> pyrolysis and oxidation in a nanosecond-pulsed discharge *Proc. Combust. Inst.* <https://doi.org/10.1016/j.proci.2020.07.095>
- [38] Hagelaar G J M and Pitchford L C 2005 Solving the Boltzmann equation to obtain electron transport coefficients and rate coefficients for fluid models *Plasma Sources Sci. Technol.* **14** 722
- [39] Pancheshnyi S, Biagi S, Bordage M C, Hagelaar G J M, Morgan W L, Phelps A V and Pitchford L C 2012 The lxcat project: electron scattering cross sections and swarm parameters for low temperature plasma modeling *Chem. Phys.* **398** 148–53
- [40] Yang X, Shen X, Santner J, Zhao H and Ju Y 2017 Princeton hp-mech. URL <http://engine.princeton.edu/mechanism/HP-Mech.html>
- [41] Garscadden A and Nagpal R 1995 Non-equilibrium electronic and vibrational kinetics in H<sub>2</sub>–N<sub>2</sub> and H<sub>2</sub> discharges *Plasma Sources Sci. Technol.* **4** 268
- [42] Guerra V, Tejero-del-Caz A, Pintassilgo C D and Alves L L 2019 Modelling N<sub>2</sub>–O<sub>2</sub> plasmas: volume and surface kinetics *Plasma Sources Sci. Technol.* **28** 073001
- [43] Gutsol A, Rabinovich A and Fridman A 2011 Combustion-assisted plasma in fuel conversion *J. Phys. D: Appl. Phys.* **44** 274001
- [44] Reuter C B, Won S H and Ju Y 2016 Experimental study of the dynamics and structure of self-sustaining premixed cool flames using a counterflow burner *Combust. Flame* **166** 125–32
- [45] Ju Y, Reuter C B, Yehia O R, Farouk T I and Won S H 2019 Dynamics of cool flames *Prog. Energy Combust. Sci.* **75** 100787

- [46] Fridman A 2008 *Plasma Chemistry* (Cambridge: Cambridge University Press)
- [47] Capitelli M, Ferreira C M, Gordiets B F and Osipov A I 2013 *Plasma Kinetics in Atmospheric Gases* vol 31 (Berlin: Springer)
- [48] Vedenov A A, Gladush G G, Griukanova L G and Samokhin A A 1980 Voltage-current characteristics of a diffusion-sustained glow discharge in a flowing gas *Sov. J. Plasma Phys.* **6** 499–504
- [49] Almeida P G C, Benilov M S, Cunha M D and Faria M J 2009 Analysing bifurcations encountered in numerical modelling of current transfer to cathodes of dc glow and arc discharges *J. Phys. D: Appl. Phys.* **42** 194010
- [50] Shkurenkov I A, Mankelevich Y A and Rakhimova T V 2009 Simulation of diffuse, constricted-stratified, and constricted modes of a dc discharge in argon: hysteresis transition between diffuse and constricted-stratified modes *Physical Review E* **79** 046406